

Article

Comparison of Microstructure, Microhardness, Fracture Toughness, and Abrasive Wear of WC-17Co Coatings Formed in Various Spraying Ways

Xiao Chen , Chengdi Li *, Qinqin Gao, Xixi Duan and Hao Liu *

Xinyu Key Laboratory of Materials Technology and Application for Intelligent Manufacturing, School of Mechanical and Electrical Engineering, Xinyu University, Xinyu 338004, China; chenxiaoxyxy@126.com (X.C.); qinqingao_2000@126.com (Q.G.); xixiduan_2001@126.com (X.D.)

* Correspondence: cdl1988_xyxy@126.com (C.L.); haol_xyxy@126.com (H.L.); Tel.: +86-790-666-6108 (C.L. & H.L.)

Abstract: WC-Co cermet materials serving as protective coatings are widely used in many fields. Conventional WC-17Co coatings were formed in high-velocity oxygen-fuel (HVOF), warm spraying (WS), and cold spraying (CS), respectively. Deposition behavior of a single WC-17Co particle, as well as the microstructure, microhardness, fracture toughness, and abrasive wear of WC-17Co coatings formed in various spraying ways were investigated. The results show that the deposition behavior of a single WC-17Co particle was different after it was deposited onto a Q235 steel substrate in various spraying ways. The WC-17Co splat deposited by HVOF showed a center hump and some molten areas, as well as some radial splashes presented at the edge of the splat. The WC-17Co splat deposited by WS presented a flattened morphology with no molten areas. However, the WC-17Co splat deposited by CS remained nearly spherical in shape and embedded into the substrate to a certain depth. All the WC-17Co coatings had the same phase compositions with that of feedstock. The microstructure of all the WC-17Co coatings was dense with no cracks or abscission phenomena between the coatings and substrate. Moreover, fine WC particles were formed in the coatings due to the fracture of coarse WC particles, and the content of fine WC particles in the cold-sprayed coating was significantly more than the other coatings. A stripe structure was formed by the slippage of fine WC particles with a plastic flow of Co binder in the warm-sprayed and cold-sprayed coatings. More fine WC particles, as well as the stripe structure, in the coatings were conducive to improve the microhardness and fracture toughness of the coating. The microhardness and fracture toughness of the cold-sprayed WC-17Co coating were the highest among the coatings. The main wear mechanism of all coatings was the groove and some peel-offs. The cold-sprayed WC-17Co coating with the lowest wear loss presented the highest wear resistance among the coatings.



Citation: Chen, X.; Li, C.; Gao, Q.; Duan, X.; Liu, H. Comparison of Microstructure, Microhardness, Fracture Toughness, and Abrasive Wear of WC-17Co Coatings Formed in Various Spraying Ways. *Coatings* **2022**, *12*, 814. <https://doi.org/10.3390/coatings12060814>

Academic Editor: Diego Martinez-Martinez

Received: 18 May 2022

Accepted: 7 June 2022

Published: 10 June 2022

Publisher's Note: MDPI stays neutral with regard to jurisdictional claims in published maps and institutional affiliations.



Copyright: © 2022 by the authors. Licensee MDPI, Basel, Switzerland. This article is an open access article distributed under the terms and conditions of the Creative Commons Attribution (CC BY) license (<https://creativecommons.org/licenses/by/4.0/>).

Keywords: WC-17Co coating; high-velocity oxygen-fuel; warm spray; cold spray; microstructure; microhardness; fracture toughness; abrasive wear

1. Introduction

WC-Co cermet materials, due to their exceptional comprehensive properties, are widely used as protective coatings of wear-resistant parts in many fields (e.g., aerospace, automobile, petrochemical, equipment manufacturing) [1–5]. Therefore, WC-Co coatings were prepared by many researchers using various spraying technologies. Thermal spraying processes, such as high-velocity oxygen-fuel (HVOF) and plasma spray, are the most frequently used technology to fabricate WC-Co cermet coatings. The microstructure and properties (e.g., mechanical, wear behavior, erosion behavior) of WC-Co coatings prepared by plasma spraying were investigated [6–10]. Studies showed that WC-Co coatings could improve the properties of the substrate, especially the coatings with a dense microstructure. However, due to the high temperature effect of plasma spraying, the decarburization and decomposition phenomena of WC ceramic phase always occurred in the as-sprayed

coatings, resulting in the formation of W , W_2C , Co_3W_3C , or Co_6W_6C phases [6–10]. Due to the low flame temperature and short residence time of particles in flame flow, the HVOF process is a favorable and feasible method to fabricate cermet coatings with excellent properties (e.g., high microhardness, low porosity, high bonding strength, and good wear resistance), especially suitable for preparing carbide cermet coatings [11,12]. Therefore, researchers have conducted a significant amount of research on the microstructure and properties of HVOF-sprayed WC-Co coatings with different WC size (e.g., conventional, fine, nanostructured, bimodal, and multimodal) and/or Co content (e.g., 10Co, 12Co, 17Co, and 25Co) [13–22]. Shipway et al. [15] reported that, due to the higher decomposition of nanostructured WC, the wear rate of conventional WC-12Co coating was lower than that of nanostructured WC-12Co coating. Cho et al. [16] also reported that, due to the denser microstructure and lower decomposition of micron WC-Co coating, the hardness and friction coefficient of micron WC-Co coating were higher than of nano WC-Co coating. Guilemany et al. [17] reported that, due to the more decarburization phenomena in the nanostructured WC-12Co coatings, the microhardness of the nanostructured WC-12Co coating was higher in comparison to bimodal and conventional WC-12Co coatings. Meanwhile, the bimodal WC-12Co coating showed a lower friction coefficient and better wear resistance than other coatings. Baumann et al. [18] reported that the fine WC-12Co coating showed the highest microhardness and wear resistance in comparison to nanostructured and conventional WC-12Co coatings. Ding et al. [3] showed that the multimodal WC-12Co coating with denser microstructure exhibited higher microhardness and better erosion resistance than submicron and conventional WC-12Co coatings. Although the WC-Co coatings could improve microhardness and wear/erosion resistance, W , W_2C , Co_3W_3C , or Co_6W_6C phases also always occurred in the HVOF-sprayed coatings [3,13–19].

A warm spraying (WS) process, as a new kind of thermal spraying technology, has been used to prepare metal (e.g., Al, Cu, and Ti etc) [21–23], Ti6Al4V [24], hydroxyapatite (HA) [25], HA/Ti [26], Ti-Al-based intermetallic coatings [27]. Meanwhile, due to the high particle temperature, which is nevertheless lower than the melting point characteristic of standard WS processes, WC-based cermet coatings were successfully deposited by warm spraying [28–32]. Chivavibul et al. [28,29] have studied the microstructure, mechanical properties, and wear resistance of WC-Co coatings with various Co contents determined by WS and HVOF processes. The results showed that the fracture toughness of warm-sprayed WC-Co coatings increased as the Co content increased, and the wear resistance of warm-sprayed WC-Co coatings was better than those of HVOF-sprayed coatings [29]. Watanabe et al. [31,32] reported that WC-Co/Cu and WC-Co/Al multilayer coatings were successfully fabricated by warm spraying. The results showed that, due to higher volume fraction of copper in WC-Co/Cu coating, the work of the fractured WC-Co/Cu coatings was higher than the monolithic WC-Co coatings, as well as the bending strength was moderately better [31]. The durability of WC-Co/Al multilayer coatings was enhanced by ductile aluminum [32]. At present, there are few reports on the research of warm-sprayed WC-Co coatings, but it can be found from existing reports that the phase compositions of WC-Co coatings prepared by warm spraying were the same as that of those powders.

Cold spraying is a kind of technology in which high velocity solid-state particles impacted into substrates to form coatings [33]. Therefore, extensive research has been done into WC-based coatings with different WC size (e.g., conventional [34–37], such as nanostructured [37–39], bimodal [40], and multimodal [41,42]) coatings fabricated by cold spraying. Couto et al. [34] reported that cold-sprayed WC-12Co and WC-17Co coatings retained the same composition phases with the original powder, and the coatings with dense microstructure showed excellent tribological and electrochemical properties. Yin et al. [35] reported that WC-Co-Ni coatings with different WC mass fractions were successfully fabricated by cold spraying, and the coating formation mechanism and tribological performance were investigated. The results showed that metallic bonding between the WC-Co and Ni particles was a possibility that occurred due to the Co phase in the WC-Co powders, and then the fine WC-17Co pieces caused by high-velocity impacting remained

in the WC-Co-Ni coating. In addition, the tribological performance of WC-Co-Ni coatings improved as the WC content increased. Li et al. [38] studied the deposition behavior of single nanostructured WC-12Co particle. The results showed that the dense nanostructured WC-12Co coating presented high microhardness (1800 Hv_{0.3}), and post-annealing treatment was beneficial to improve the bonding between deposited nanostructured WC-12Co particles and the toughness of the coatings. Yang et al. [40] reported that cold-sprayed WC-(nanoWC-Co) coatings showed higher microhardness and toughness, as well as much higher wear resistance by comparing with HVOF-sprayed conventional WC-Co coatings. In addition, the post-spray annealing treatment could improve the toughness of the coating, especially the wear resistance. Ji et al. [42] reported that the mechanical and abrasive wear properties were influenced by the content of nano WC-17Co particles in the multimodal WC-17Co feedstocks. And the abrasive wear mechanism of multimodal WC-17Co was also investigated.

In recent years, there are few reports on the preparation of WC-Co coatings by various spraying ways. Hence, in order to investigate the effects of various spraying methods on the deposition behavior of a single WC-17Co particle, as well as the microstructure, mechanical, and abrasive wear properties of the coatings, WC-17Co coatings were fabricated by HVOF, WS, and CS technologies in this study. The main innovations of this study are as follows: (1) contrastive analysis is applied to the deposition behavior of a single WC-17Co particle across various spraying methods; (2) the warm-spraying technology is applied to fabricate WC-17Co coating; (3) the decomposition and decarburization of WC are restrained by controlling the HVOF processing parameters; (4) the contrastive analysis on the microstructure, microhardness, fracture toughness, and abrasive wear properties of WC-Co coatings prepared by various spraying methods is investigated.

2. Materials and Methods

2.1. Materials

Raw materials used in this study were commercially available conventional WC-17Co powders with WC size of 0.2–2 μm (Ganzhou Zhangyuan Tungsten Advance Material Co., Ltd., Ganzhou, China). An agglomeration sintering method was used to manufacture these powders. The surface and cross-section morphologies of WC-17Co powders were shown in Figure 1. The size distribution of WC-17Co powders analyzed by a laser diffraction meter (GSL-1020, Liaoning Instrument Research Institute Co., Ltd., Liaoning, China) was shown in Figure 2. The size distribution (D10, D50, and D90) of powders was 19.5 μm, 29.6 μm, and 44.6 μm, respectively. Q235 steel with dimensions of 50 mm × 25 mm × 3 mm was used as a substrate for depositing single WC-17Co coatings. Prior to spraying, Q235 steel substrate was pre-cleaned by acetone for 10 min in ultrasonic cleaner, and then grit blasted by aluminum oxide of 700 μm to achieve a roughened surface for improving the bonding strength between the coating and substrate.

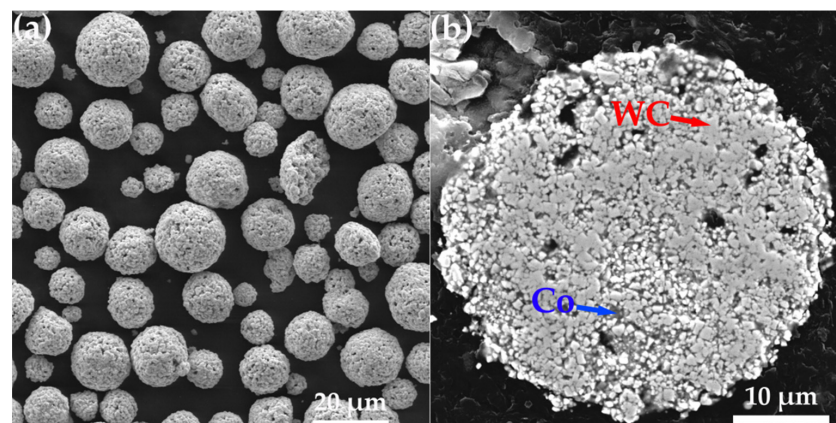


Figure 1. The morphologies of WC-17Co powder (a) surface, 2000×, (b) cross-section, 5000×.

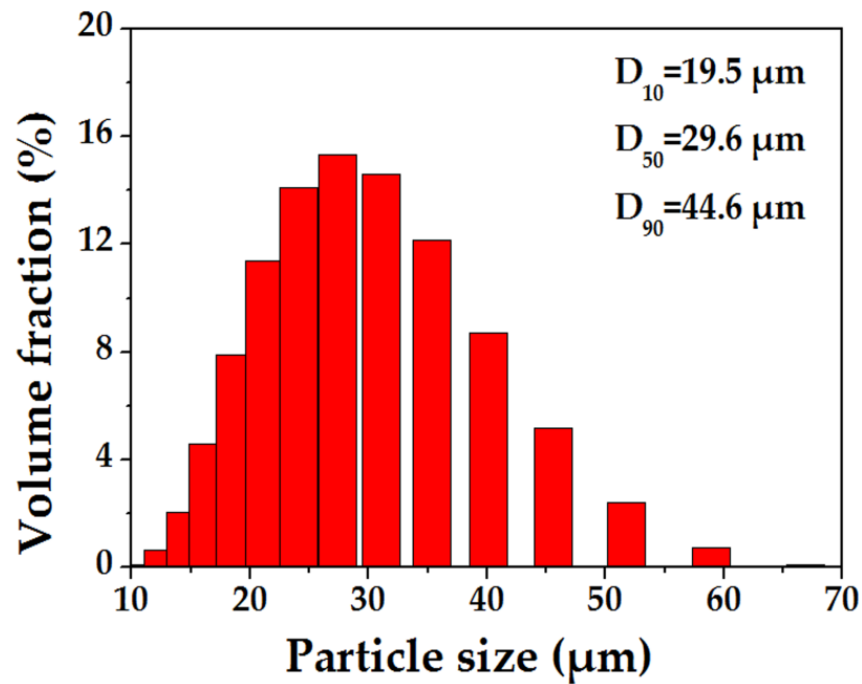


Figure 2. The particle size distribution of WC-17Co powders.

2.2. Coating Preparation

HVOF, WS, and CS equipment adopted a home-made high-velocity oxygen fuel spray system (CH-2000, Xi'an Jiaotong University, Shanxi, China), a modified high-velocity oxygen fuel spray system (CH-2000, Xi'an Jiaotong University, Shanxi, China), and a home-made cold-spray system (CS-2000, Xi'an Jiaotong University, Shanxi, China), respectively. Nitrogen gas was used as an auxiliary gas to adjust the flame temperature for warm spraying in this study. A schematic diagram of HVOF and WS spray systems is illustrated in Figure 3, and a schematic diagram of CS spraying system is illustrated in Figure 4. The detail parameters of as-sprayed WC-17Co coatings are listed in Table 1. Spraying powder feeding adopted a scraper powder feeder (Guangzhou Sanxin Metal S & T Co., Ltd., Guangzhou, China).

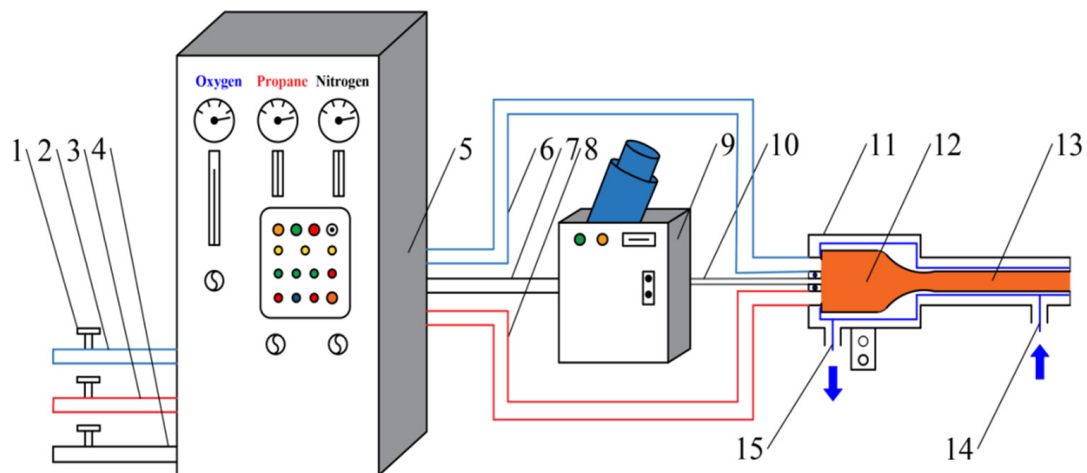


Figure 3. Schematic diagram of HVOF and WS spray system: (1) valve, (2,6) oxygen pipe, (3,8) propane pipe, (4,7) nitrogen pipe, (5) console cabinet, (9) powder feeder, (10) powder feeding pipe, (11) spray gun, (12) flame chamber, (13) spraying tube, (14) cold water inlet, and (15) cold water outlet.

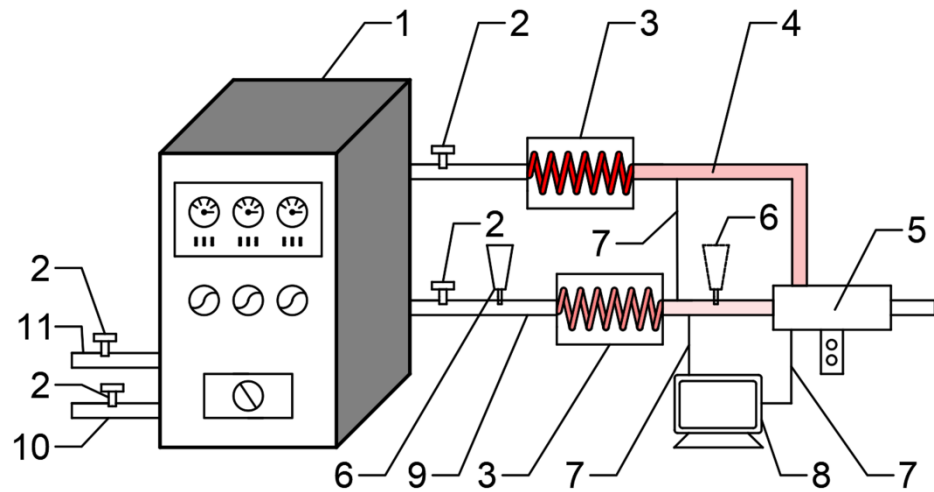


Figure 4. Schematic diagram of cold-spray system: (1) console cabinet, (2) Valve, (3) gas heater, (4) accelerating gas pipe, (5) spray gun, (6) powder feeder, (7) thermal couples, (8) display panel, (9) carrier gas, (10) powder feeder gas inlet, (11) accelerating gas inlet.

Table 1. The detail spraying parameters of as-sprayed WC-17Co coatings.

HVOF Spray	Value	Warm Spray	Value	Cold Spray	Value
Pressure of O ₂ /MPa	0.55	Pressure of O ₂ /MPa	0.55	Accelerating gas pressure/MPa	2.4
Flow rate of O ₂ /L·min ⁻¹	543	Flow rate of O ₂ /L·min ⁻¹	543	Powder-feeding gas pressure/MPa	2.6
Pressure of C ₃ H ₈ /MPa	0.4	Pressure of C ₃ H ₈ /MPa	0.4	Gas temperature in gun chamber/°C	750 ± 30
Flow rate of C ₃ H ₈ /L·min ⁻¹	24	Flow rate of C ₃ H ₈ /L·min ⁻¹	24		
Pressure of N ₂ /MPa	0.6	Pressure of N ₂ /MPa	0.6		
Flow rate of N ₂ /L·min ⁻¹	45	Flow rate of N ₂ /L·min ⁻¹	450		
Transverse speed of gun/mm·s ⁻¹	150	Transverse speed of gun/mm·s ⁻¹	100	Transverse speed of gun/mm·s ⁻¹	10
Spray distance/mm	200	Spray distance/mm	200	Spray distance/mm	20
Rotation rate/r·min ⁻¹	50	Rotation rate/r·min ⁻¹	50	Rotation rate/r·min ⁻¹	50
coats of powder	20	coats of powder	20	coats of powder	20
Substrate	Q235 steel	Substrate	Q235 steel	Substrate	Q235 steel

2.3. Microhardness, Fracture Toughness and Abrasive Wear

Vickers microhardness tests were performed on the polished cross-section of as-sprayed WC-17Co coatings, and the equipment used included a digital microhardness tester (HXD-1000 TM/LCD, Shanghai Precision Instruments Co., Ltd., Shanghai, China) under a load of 2.94 N for a dwell time of 20 s. The average value of ten random measurements was used as the final microhardness. A Vickers indentation technique was used to evaluate the plain strain fracture toughness (i.e., K_{IC}) of as-sprayed WC-17Co coatings at 5 kgf load and 20 s dwell time. Fracture toughness (K_{IC}) was calculated by applying the following equation proposed by Niihara [43]:

$$K_{IC} = 0.0193(H_v d) \left(\frac{E}{H_v} \right)^{2/5} (a)^{-1/2} \tag{1}$$

where, K_{IC} is the fracture toughness, H_v is the Vickers hardness, d is the half-diagonal of the Vickers indentation, E is the elastic modulus, and a is the indentation crack length.

The elastic modulus of the coatings was determined according to the following formula as established in [44]:

$$\left(\frac{b'}{a'}\right) = \left(\frac{b}{a}\right) - \alpha\left(\frac{H_v}{E}\right) \quad (2)$$

where, a and b are the diagonal dimensions of Knoop indenter, a' and b' are the long and short diagonal dimensions measured on residual Knoop indentation impression, α is a constant equal to 0.45, H_v is the Vickers hardness.

The abrasive wear test was carried out by a pin-on-disk method. The detail of the preparation for wear specimens can be found in the literature, namely [45]. The schematic diagram of abrasive wear test was shown in Figure 5. The wear parameters of as-sprayed WC-17Co are listed in Table 2.

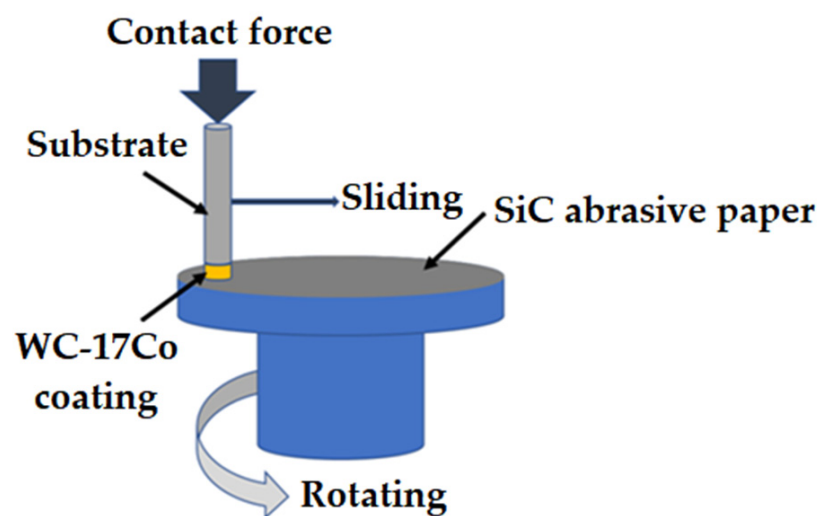


Figure 5. Schematic diagram of abrasive wear test.

Table 2. The wear parameters of as-sprayed WC-17Co coatings.

Wear Parameters	Values
Load/N	10
Rotation speed of the disk/ $r \cdot \text{min}^{-1}$	60
Radial feed rate of the pin/ $\text{mm} \cdot \text{r}^{-1}$	4
Wear distance/m	16
SiC abrasive paper	300 grit size

2.4. Microstructure Characterization of Powders and Coatings

A test involving a scanning electron microscope (SEM; VEGA II-LSU, TESCAN, Brno, Czech Republic) was performed on the samples to characterize the morphologies of feedstock powders, deposited splats, coatings cross-section, and worn surface in backscattering electron (BSE) mode. The elemental composition of single WC-17Co splat was analyzed by electron dispersive x-ray spectroscopy (EDS; VEGA II-LSU, TESCAN, Brno, Czech Republic). X-ray diffraction (XRD; Bruker D8 Advance, Karlsruhe, Germany) was conducted for the phase compositions of feedstock powders and as-sprayed coatings with $\text{Cu-K}\alpha$ radiation ($\lambda = 1.5418 \text{ \AA}$, 35 kV, and 35 mA) for the scanning range (2θ) of $20\text{--}90^\circ$ with a step of 0.02° and a scanning speed of $10^\circ/\text{min}$. Figure 6 shows the XRD patterns of conventional WC-17Co powders. The average porosity and thickness of conventional WC-17Co coatings were calculated by the image-analysis method (Software Image J, version 1, National Institutes of Health, Bethesda, MD, USA) with ten SEM micrographs from cross-section morphologies and backscattered electron (BSE) microscopies.

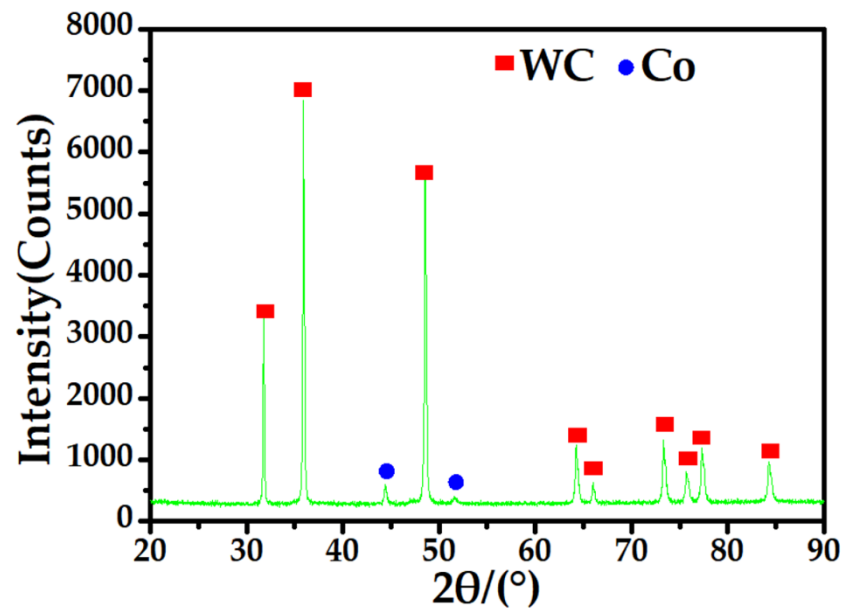


Figure 6. The X-ray diffraction (XRD) patterns of conventional WC-17Co powders.

3. Results and Discussion

3.1. Deposition Behavior of WC-17Co Splats

Figure 7 shows the surface morphologies of the WC-17Co splats deposited in various spraying methods. It can be seen that a WC-17Co splat deposited by HVOF showed a center hump (marked in cyan dot circle in Figure 7a), and some radial splashes (as indicated by the green arrow in Figure 7a) presented at the edge of the splat. Meanwhile, there were also observed some molten areas (as indicated by the yellow arrow in Figure 7a) in the WC-17Co splat, while the WC-17Co splat deposited by WS presented a typical pie shape morphology with no molten areas. However, due to the plastic deformation of the WC-17Co splat, some cracks (as indicated by the black arrow in Figure 7b) occurred on the surface of the splat, and an obvious ripple (as indicated by the orange arrow in Figure 7b) appeared around the splat, contributing to the cooperative deformation of the substrate. The morphology of the WC-17Co splat deposited by CS still remained nearly spherical in shape, which was the same as that of the original feedstock powders. Due to the high-velocity impacting effect of cold-sprayed splat, some cracks (as indicated by the black arrow in Figure 7c) also appeared on the surface of the large cold-sprayed WC-17Co splat. In addition, compared to the analysis results of the warm-sprayed WC-17Co splat, the plastic deformation of the substrate was more severe after cold spraying, more ripple (as indicated by the orange arrow in Figure 7c) and revers (as indicated by the purple arrow in Figure 7c) phenomena appeared around the splat. Moreover, there appeared gaps (as indicated by green arrow in Figure 7c) between the splat and the substrate. Meanwhile, it can be further observed that the embedding depth of the small splat into Q235 steel substrate was deeper than that of the large splat (as shown in Figure 8).

3.2. XRD Patterns of As-Sprayed WC-17Co Coatings

Figure 9 shows the XRD patterns of WC-17Co coatings as-sprayed in various spraying ways. It can be found that, although there was a small amount of W_2C phase in HVOF-sprayed coating, the main phase compositions of all WC-17Co coatings were WC and Co phases. This illustrates that, the decomposition and decarburization of WC could be effectively inhibited by controlling HVOF process parameters; however, the W_2C phase also formed at a certain high-spraying temperature of HVOF. Meanwhile, due to the low temperature effect of WS and CS, the phase compositions of WC-17Co powders were transplanted into warm-sprayed and cold-sprayed coatings [46]. When comparing the warm-sprayed and cold-sprayed coatings to HVOF-sprayed WC-17Co coatings, it also

can be further found that the diffraction peaks of WC and Co of warm-sprayed and cold-sprayed WC-17Co coatings were broader. Lima et al. [47] reported that residual stresses and grain refinement are the main factors that induce the peak broadening, and the residual stress is often caused by high temperatures during spraying. Ji et al. [41] also reported that, in the cold spraying process, grain refinement is the main reason for the peak broadening of WC, and the effect of residual stress is negligible. Therefore, due to the control of the HVOF process parameters for reducing the flame temperature in this study, residual stress had little influence on the WC-17Co coating. Figure 10 shows the full widths at half maximums (FWHMs) of WC and Co diffraction peaks of WC-17Co coatings formed in various spraying ways. It can be found that the FWHMs of WC and Co diffraction peaks of warm-sprayed and cold-sprayed WC-17Co coatings were larger than those of HVOF-sprayed coatings; in addition, those of cold-sprayed WC-17Co coatings were the largest. This illustrates that plastic deformation degree of incident WC-17Co particles with lower spraying temperature, such as warm spraying and cold spraying, was larger than that of WC-17Co particles deposited by HVOF. In addition, due to the high-velocity characteristic of cold spraying, the incident WC-17Co particles could be fragmented to more fine particles after impacting onto Q235 steel substrate or pre-deposited layer. Therefore, the diffraction peaks of WC and Co of cold-sprayed WC-17Co coatings were more broadened than those of warm-sprayed WC-17Co coatings.

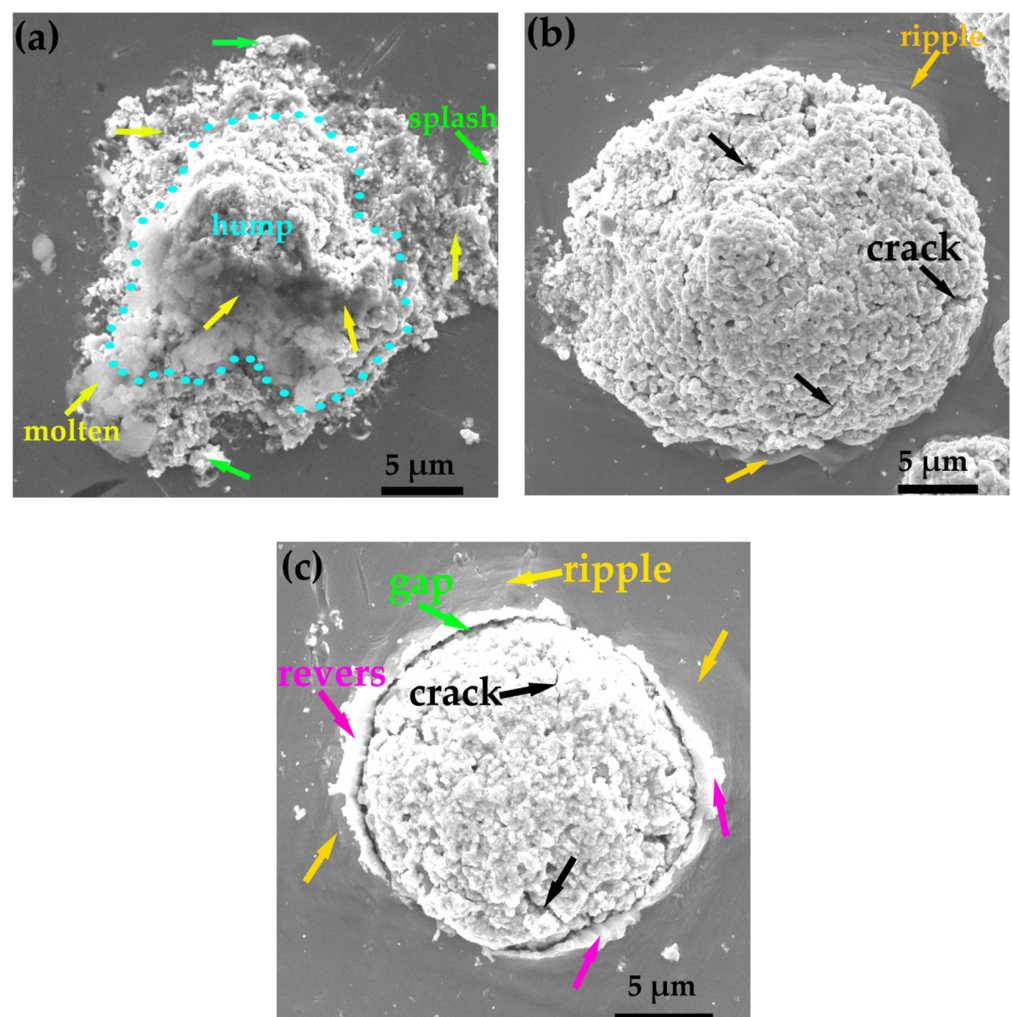


Figure 7. Surface morphologies of WC-17Co splats deposited by various spraying methods (a) HVOF, (b) WS, (c) CS.

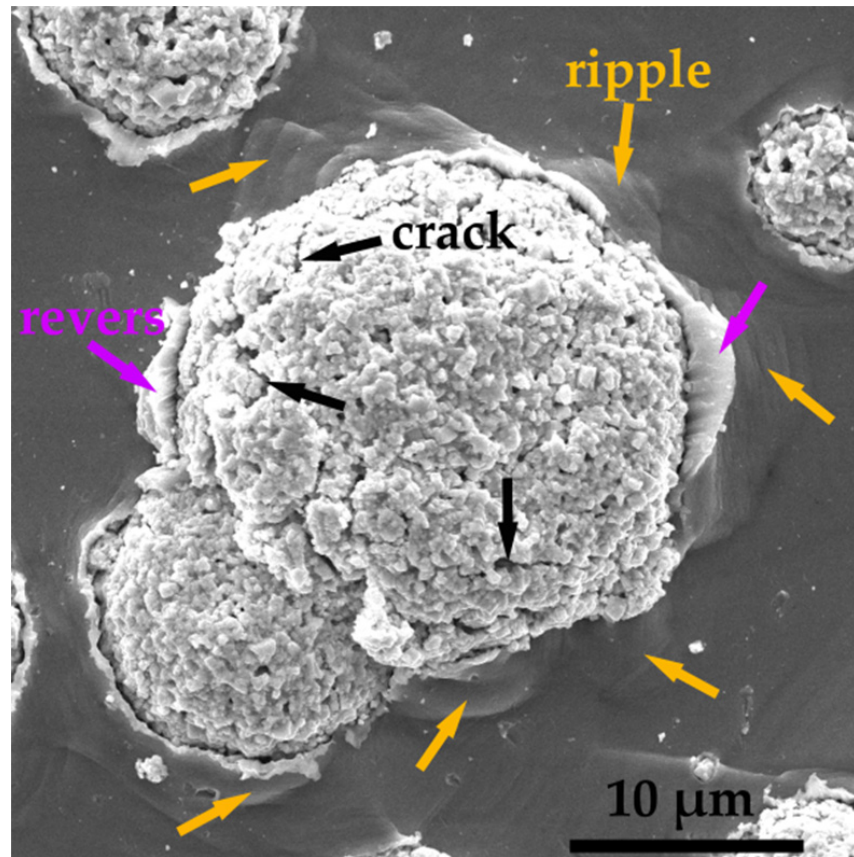


Figure 8. Surface morphologies of different size WC-17Co splats deposited by cold spraying.

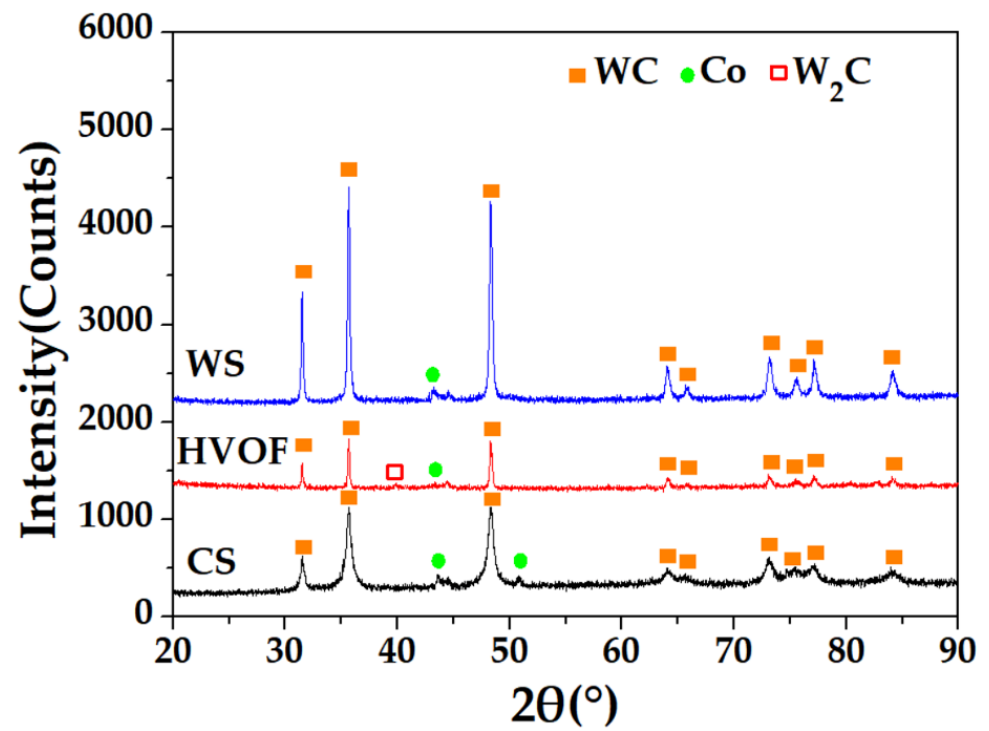


Figure 9. XRD patterns of WC-17Co coatings formed in various spraying ways.

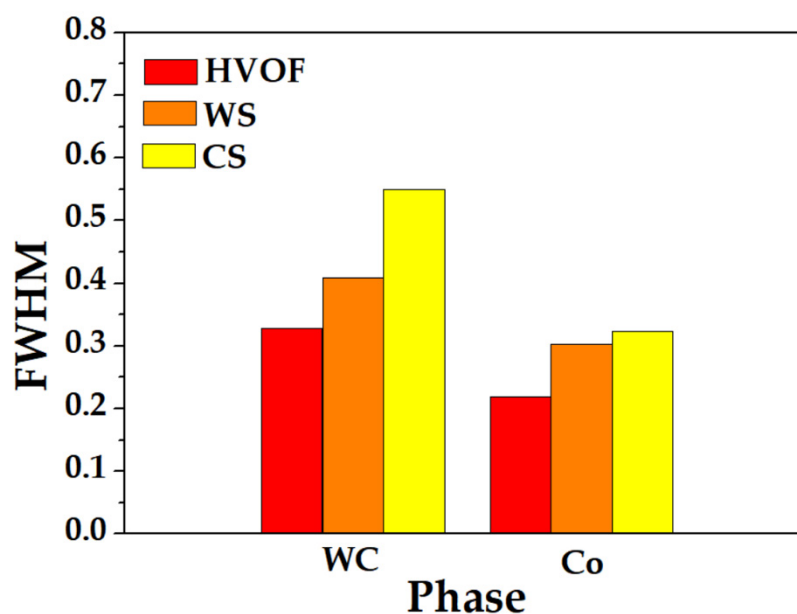


Figure 10. Full widths at half maximum (FWHMs) of WC and Co in WC-17Co coatings formed in various spraying ways.

3.3. Microstructure of As-Sprayed WC-17Co Coatings

Figure 11 shows the cross-section morphologies of WC-17Co coatings formed by various spraying methods. It can be seen that there were no cracks or abscission phenomena occurred between the coating and substrate (as shown in Figure 11b,d,f). Further analysis of the morphologies of WC-17Co coatings (as shown in Figure 11a,c,e) found that the interface between WC and Co in all WC-17Co coatings was well-bonded. Meanwhile, the content of fine WC particles (as indicated by the red arrow in Figure 11a,c,e) in the cold-sprayed coating was significantly more than the other coatings. The size range of fine WC particles formed in HVOF, WS, and CS was about 0.11–0.16 μm , 0.10–0.13 μm , 0.09–0.12 μm , respectively. It was also further indicated that more fragmented phenomenon of coarse WC particles occurred in the cold-sprayed WC-17Co coatings. These phenomena are consistent with the phase compositions analysis and results of WC-17Co coatings. By measuring the mean porosity and thickness of WC-17Co coatings formed in various spraying ways, it was found that the mean porosity of WC-17Co coatings formed in HVOF, WS, and CS was 1.57%, 0.89%, and 0.058%, respectively (as shown in Figure 12). In general, the microstructure of all coatings is dense; however, the porosity of warm-sprayed and cold-sprayed WC-17Co coatings was lower than that of HVOF-sprayed coating, and the porosity of cold-sprayed coating was the lowest. The main reasons for this phenomenon were attributed to solid-state particles' continuous impact and compaction on the warm-sprayed or cold-sprayed WC-17Co coatings at the lower spraying temperature. Meanwhile, stripe structure (as indicated by the yellow arrow in Figure 11c,e) formed by the slippage of fine WC particles with a plastic flow of Co binder could fill the pores in the warm-sprayed or cold-sprayed WC-17Co coatings [41]. Therefore, due to the cold spraying high-velocity characteristic and more stripe structure in the cold-sprayed coating, the porosity of cold-sprayed WC-17Co coating was the lowest among all the coatings. The mean thickness of WC-17Co coatings formed in HVOF, WS, and CS was $544.33 \pm 4.81 \mu\text{m}$, $528.75 \pm 5.98 \mu\text{m}$, and $207.61 \pm 9.64 \mu\text{m}$, respectively (as shown in Figure 13). Figure 14 shows the morphologies of WC-17Co particles deposited onto Q235 steel substrate surface in various spraying ways. It can be found that craters were formed as the incident particles rebounding from the Q235 steel substrate surface (as indicated by white arrow in Figure 14). The ratio of WC-17Co splats (as indicated by black arrow in Figure 14) adhered on the Q235 steel substrate surface in HVOF, WS, and CS was 54.66%, 50.18%, and 30.12%, respectively. This illustrates that decreasing the spraying temperature resulted in more content of the craters caused by

particles rebounding from the substrate surface. Therefore, this result also revealed that, although the porosity of cold-sprayed WC-17Co coating was the lowest in this study, more rebounding-particles phenomena presented during cold spraying process led to the lowest thickness of the cold-spraying coating among all the coatings.

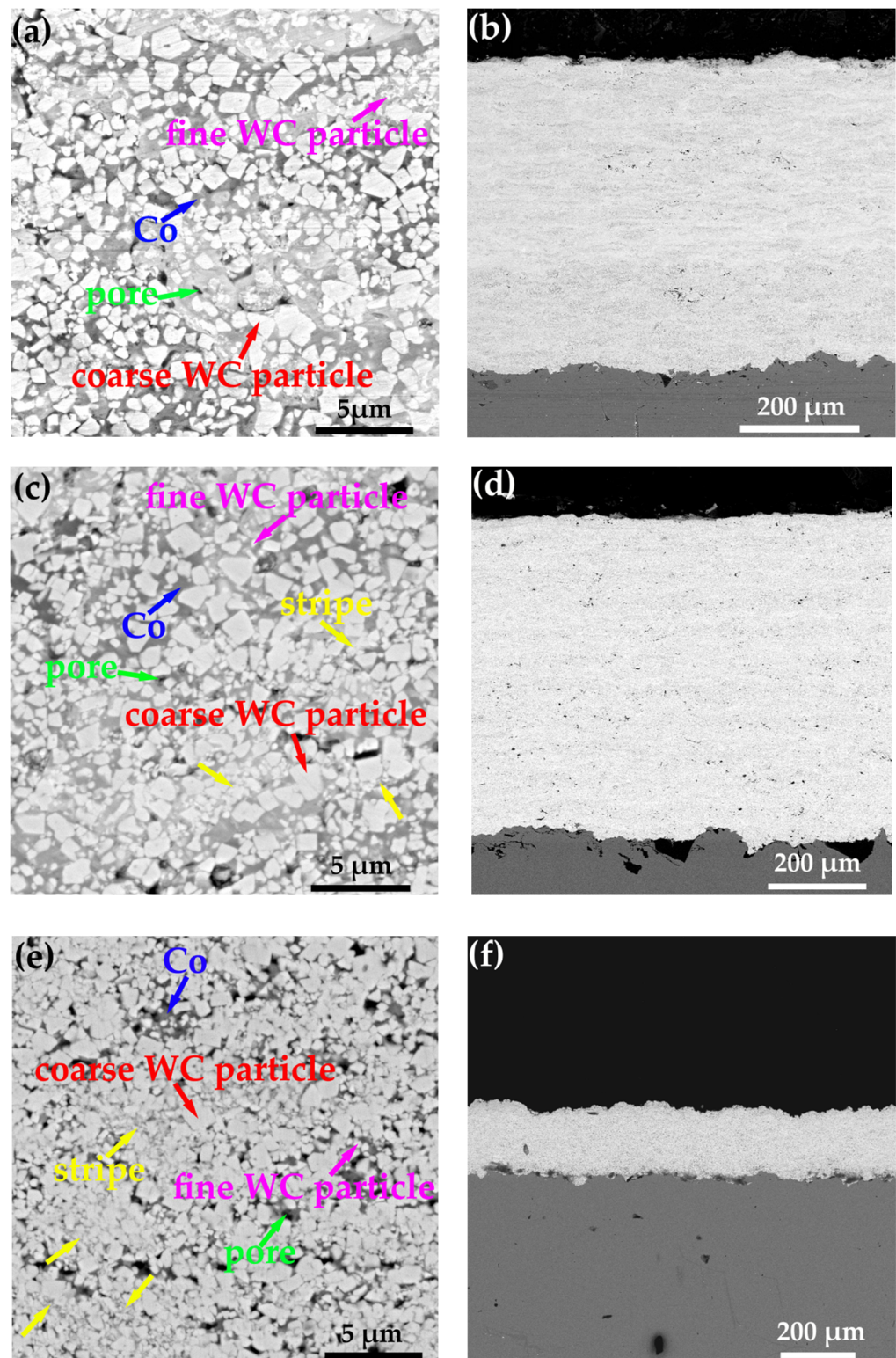


Figure 11. Cross-section morphologies of WC-17Co coatings formed by various spraying methods (a,b) HVOF, (c,d) WS, (e,f) CS.

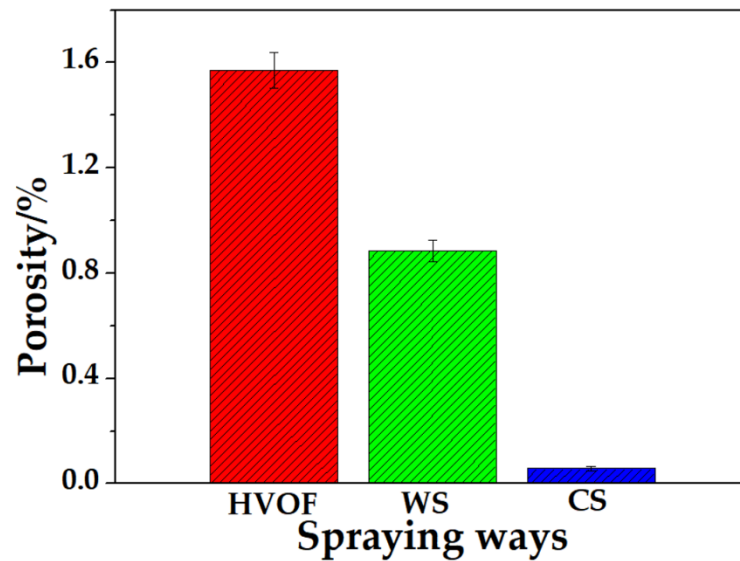


Figure 12. Porosity of WC-17Co coatings formed by various spraying methods.

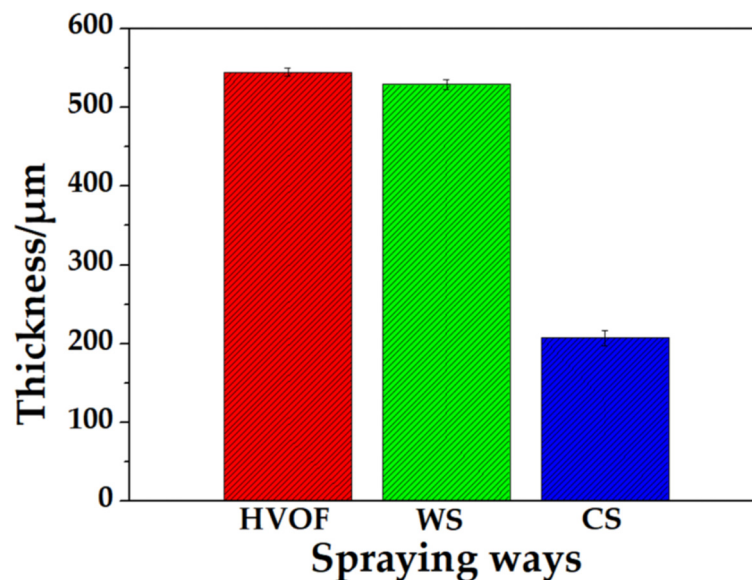


Figure 13. Thickness of WC-17Co coatings formed by various spraying methods.

3.4. Microhardness and Fracture Toughness of As-Sprayed WC-17Co Coatings

The average microhardness of WC-17Co coatings formed in HVOF, WS, and CS was 980.0 ± 17.6 HV_{0.3}, 1034.8 ± 57.5 HV_{0.3}, and 1136 ± 26.8 HV_{0.3}, respectively (as shown in Figure 15). It can be found that the average microhardness of the cold-sprayed WC-17Co coating was the highest among all the coatings. Although the W₂C phase in the coating could affect the hardness significantly [29], the content of W₂C phase was very low in the HVOF-sprayed WC-17Co coating in this study. Hence, the influence of W₂C phase on the hardness in this study was slight. Ji et al. [41] reported that stripe microstructure could enhance the spreading or flattening of WC-Co particles and improve the microstructure and microhardness of the coatings. Wang et al. [42] also reported that high content of nano WC and high density could increase the microhardness of cold-sprayed multimodal WC-12Co coatings. Therefore, combined with the microstructure analysis results of warm-sprayed or cold-sprayed WC-17Co coatings in this study, fine WC particles were formed based on the combined action of particles impacting on the substrate or pre-deposited layer and continuous impacting of incident particles. Meanwhile, a stripe structure was

formed by the slippage of fine WC particles with a plastic flow of Co binder; in particular, a stripe structure was more prevalent in cold-sprayed coatings. Therefore, the average microhardness of cold-sprayed WC-17Co coating was the highest. The average fracture toughness of WC-17Co coatings formed in HVOF, WS, and CS was 8.88 ± 0.31 , 10.42 ± 0.28 , and 13.18 ± 0.49 $\text{MPa}\cdot\text{m}^{-1/2}$, respectively (as shown in Figure 16). The Vickers indentation cracks of as-sprayed WC-17Co coatings were shown in Figure 17. Lee et al. [48] reported that decreasing powder size or the mixing ratio of the coarse WC particles could increase the fracture toughness of the coatings. Chen et al. [49] reported that W_2C phase could decrease the fracture toughness of the coating. Therefore, the fracture toughness of cold-sprayed WC-17Co coating was the highest among all the coatings in this study. This also illustrates that the fracture toughness increased with increasing the content of fine WC particles and stripe structure.

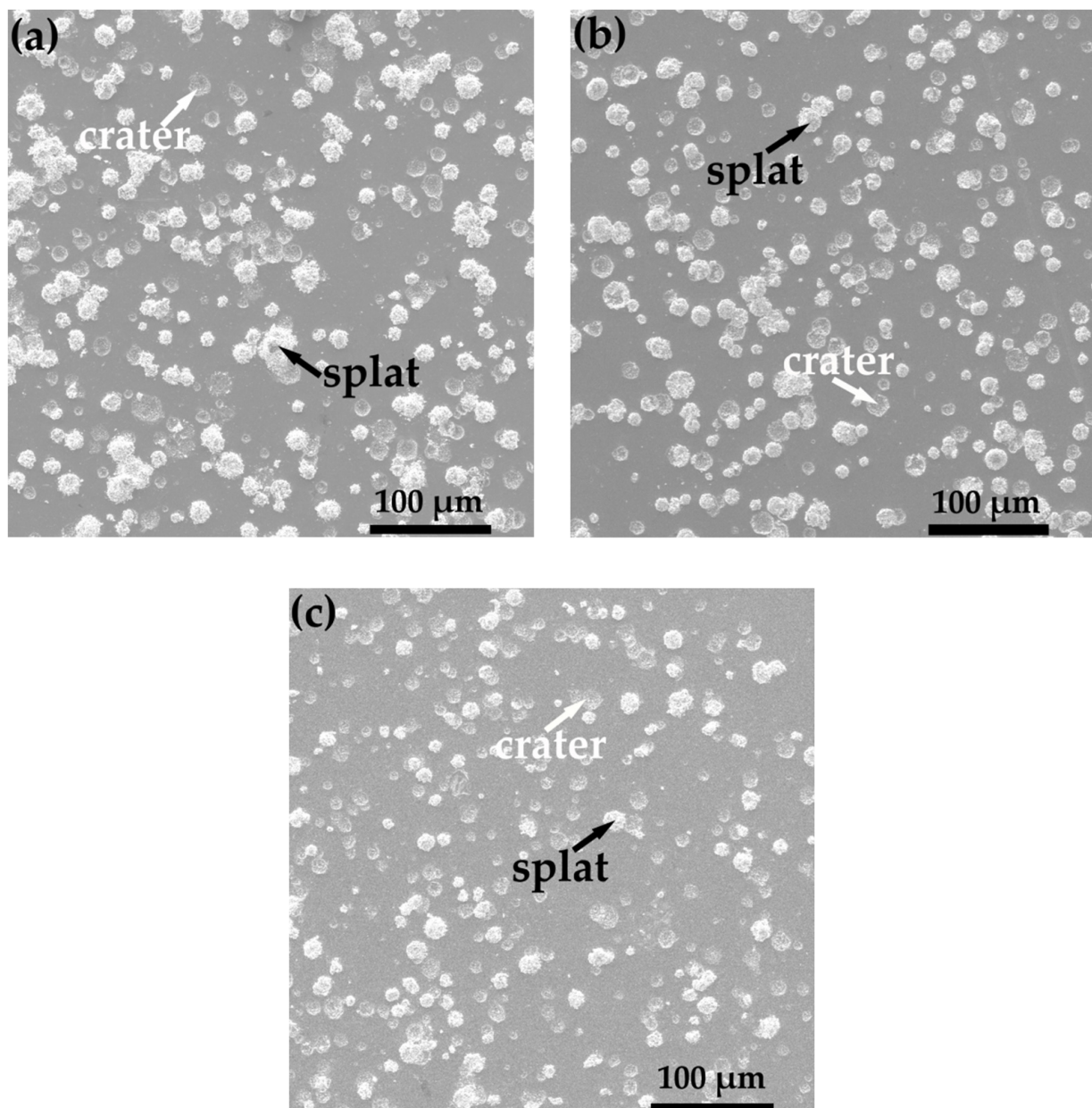


Figure 14. Morphologies of WC-17Co particles deposited onto Q235 steel substrate in various spraying ways (a) HVOF, (b) WS, (c) CS.

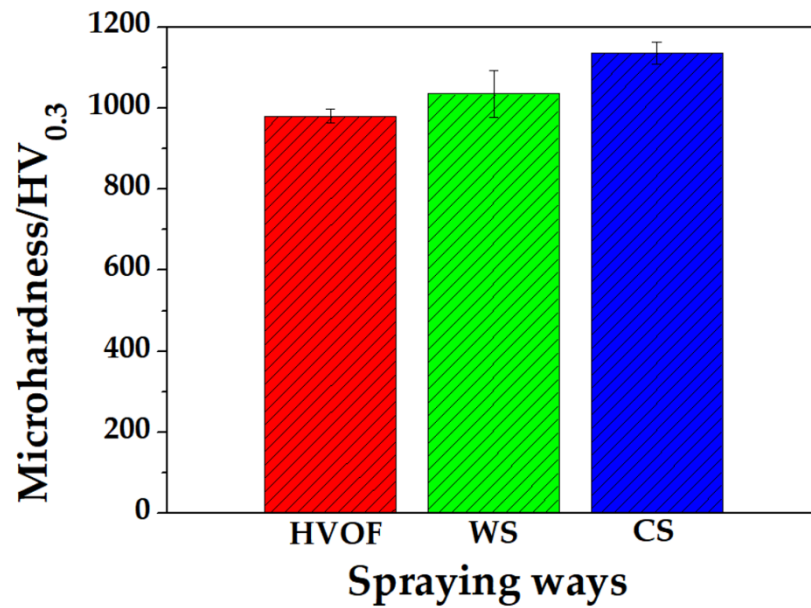


Figure 15. Microhardness of WC-17Co coatings formed by various spraying methods.

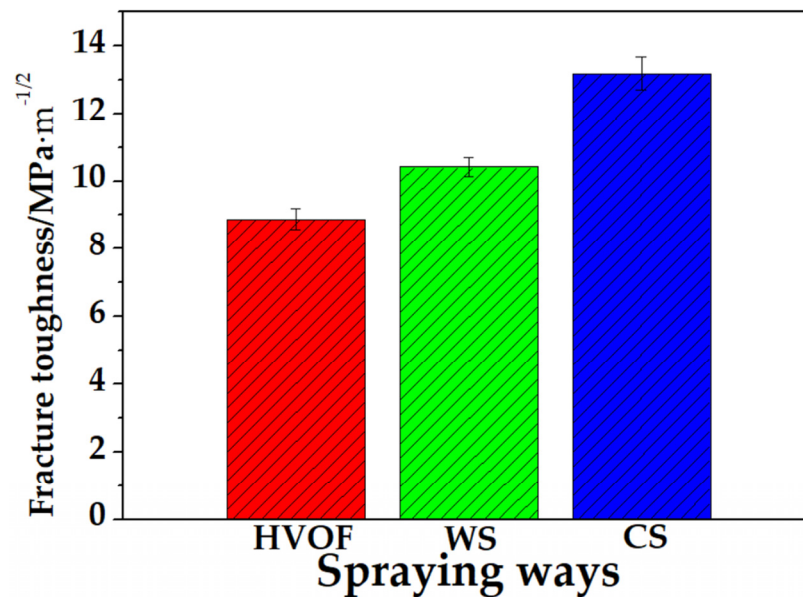


Figure 16. Fracture toughness of WC-17 coatings formed by various spraying methods.

3.5. Abrasive Wear of As-Sprayed WC-17Co Coatings and Q235 Steel

The worn surface morphologies of WC-17Co coatings formed in various spraying ways and Q235 steel substrate were shown in Figure 18. It can be seen that the main wear mechanism of all coatings was the groove (as indicated by the cyan arrow in Figure 18a,c,e) and some peel-offs (as indicated by the white arrow in Figure 18a,c,e), but the worn surface of Q235 steel was only wide and deep groove (as indicated by the cyan arrow in Figure 18g). The main reasons for the peel-off phenomenon in this study were that the crack formation (as indicated by the black arrow in Figure 18a) caused by the fracture of coarse WC particles resulted in WC particles pulled-out from the worn surface, or the exposed WC particles peeled off due to the poor bonding between WC particle and Co binder after the removal of soft Co matrix. Furthermore, in contrast to HVOF sprayed and warm-sprayed WC-17Co coatings, the grooves of cold-sprayed coating were smoother and shallower (as shown in Figure 18f). The reason for this phenomenon was that, according to the microstructure

analysis of the cold-sprayed WC-17Co coating (as shown in Figure 11e), more fine WC particles and stripe structures presented in cold-sprayed WC-17Co coatings; fine WC particles uniformly distributed into the Co binder phase, resulting in an increase in the wear resistance of the coating. Figure 19 shows the average weight loss of WC-17 coatings formed in various spraying ways and Q235 steel substrate. The average weight loss of WC-17Co coatings formed in HVOF, WS, and CS was 8.15 ± 0.31 mg, 5.31 ± 0.32 mg, and 4.05 ± 0.41 mg, respectively. This also illustrates that combining with the results analysis of the microstructure, mechanical properties, and worn surface morphologies of the coatings, the cold-sprayed WC-17Co coating presented the lowest wear loss among all the coatings. However, the average weight loss of Q235 steel substrate was 21.77 ± 0.25 mg, which was more than 5 times that of the cold-sprayed WC-17Co coating.

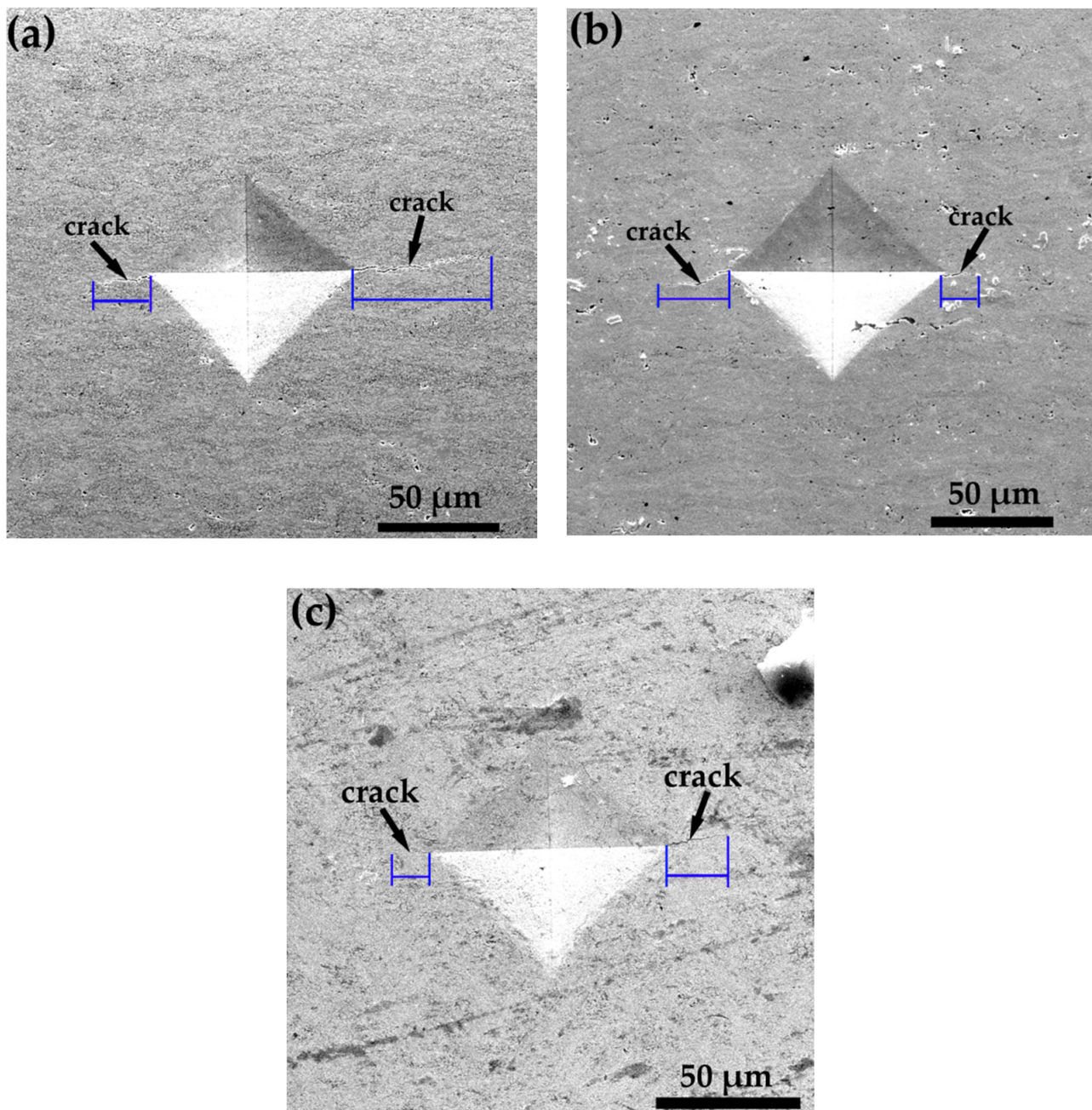


Figure 17. Vickers indentation morphologies of WC-17 coatings formed in various spraying ways (a) HVOF, (b) WS, (c) CS.

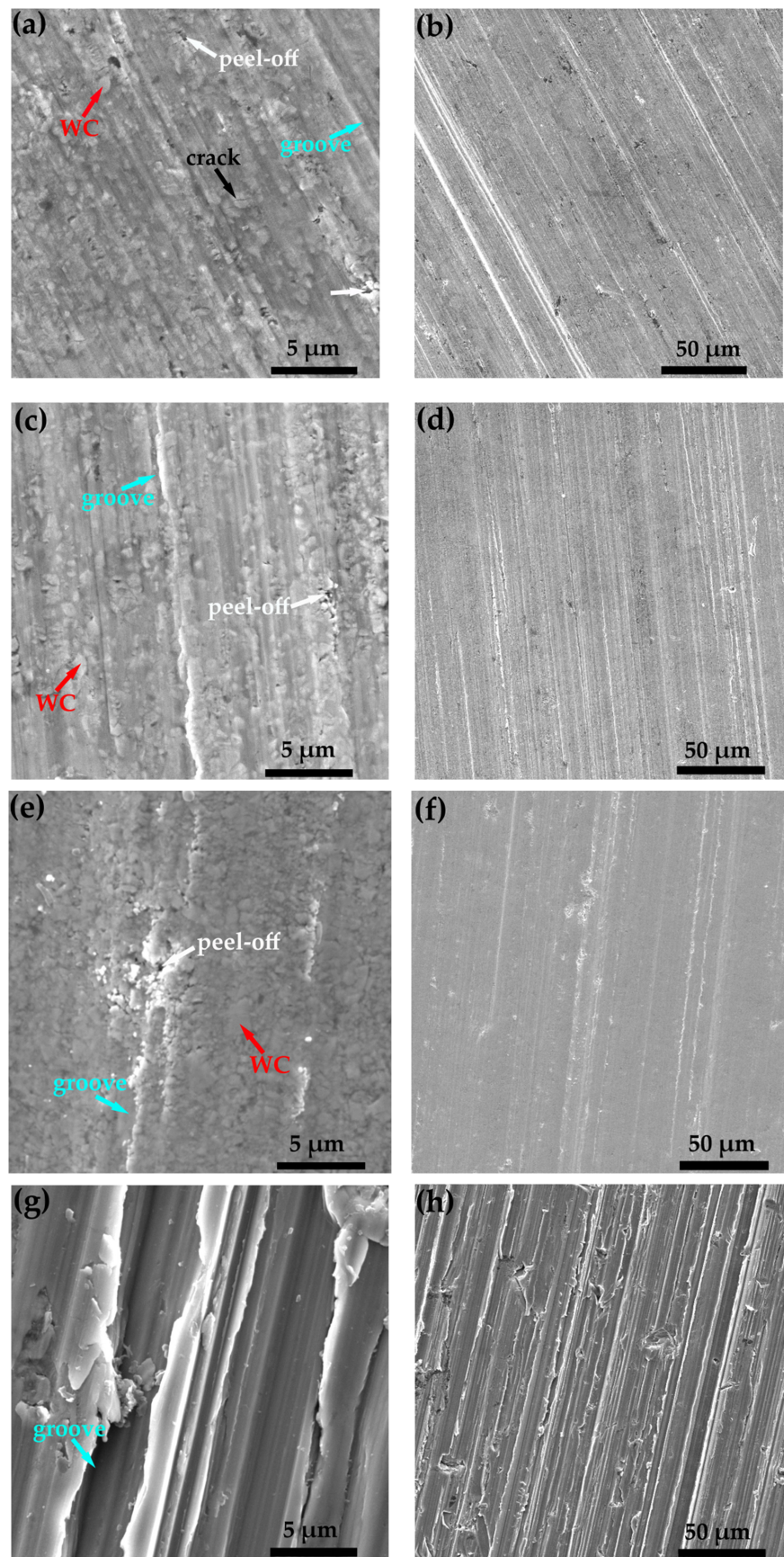


Figure 18. Worn surface morphologies of WC-17 coatings formed by various spraying methods and Q235 steel substrate (a,b) HVOF, (c,d) WS, (e,f) CS, (g,h) Q235 steel substrate.

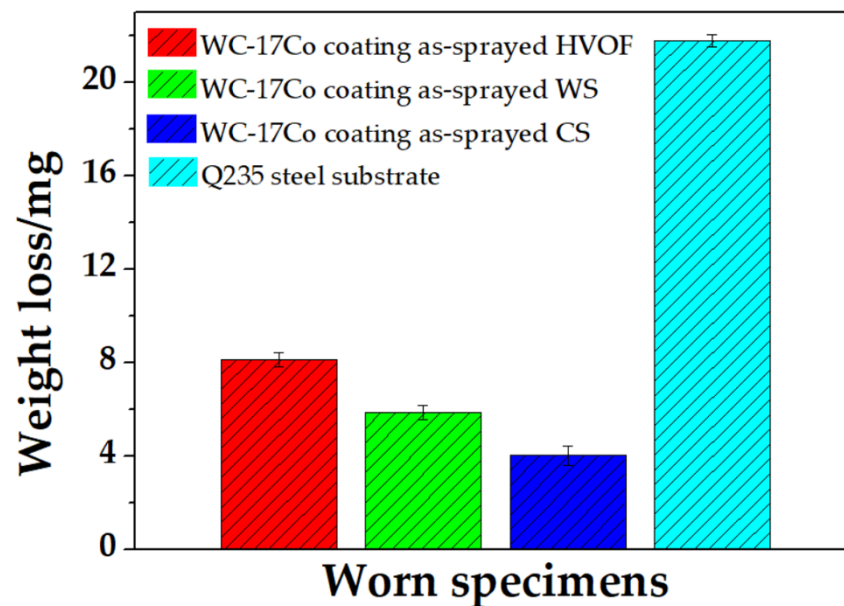


Figure 19. Weight loss of WC-17 coatings formed by various spraying methods and Q235 steel substrate.

4. Conclusions

Conventional WC-17Co powder was deposited onto Q235 steel substrate by various spraying methods to form different WC-17Co coatings. The deposition behavior of single WC-17Co particles, as well as the comparison of microstructure, microhardness, fracture toughness and abrasive wear of as-sprayed WC-17Co coatings, were investigated in this study. The main conclusions are as follows:

- I. In comparison to the WC-17Co splat deposited by HVOF and WS, the WC-17Co splat deposited by CS remained nearly spherical shape, and the embedding depth of the small particle into Q235 steel substrate was deeper than that of large splat. Due to the high-velocity impacting effect of cold-sprayed splat, the plastic deformation of the substrate was severe with more ripple and revers.
- II. Although there was a small amount of W_2C phase in HVOF-sprayed coating, the main phase compositions of all the WC-17Co coatings were WC and Co phases. By comparing with HVOF-sprayed WC-17Co coating, the diffraction peaks of WC and Co of warm-sprayed and cold-sprayed WC-17Co coatings were broadened. By measuring the full widths at half maximums (FWHMs) of WC and Co diffraction peaks of WC-17Co coatings formed in various spraying ways, the FWHMs of WC and Co diffraction peaks of warm-sprayed and cold-sprayed WC-17Co coatings were larger than those of HVOF-sprayed coatings; moreover, those of the cold-sprayed WC-17Co coatings were the largest.
- III. Due to the fragment of coarse WC particles, fine WC particles were observed in the coatings; in particular, the content of fine WC particles in the cold-sprayed coating was the highest. The size range of fine WC particles formed in HVOF, WS, and CS was about 0.110.16 μm , 0.10–0.13 μm , 0.09–0.12 μm , respectively. Due to the cold spraying high-velocity characteristic and more stripe structures in the cold-sprayed coating, the microstructure of the cold-sprayed coating was denser than the other coatings. The mean porosity of WC-17Co coatings formed in HVOF, WS, and CS was 1.57%, 0.89%, and 0.058%, respectively. The mean thickness of the WC-17Co coatings formed in HVOF, WS, and CS was $544.33 \pm 4.81 \mu\text{m}$, $528.75 \pm 5.98 \mu\text{m}$, and $207.61 \pm 9.64 \mu\text{m}$, respectively.
- IV. The average microhardness of the WC-17Co coatings formed in HVOF, WS, and CS was $980.0 \pm 17.6 \text{HV}_{0.3}$, $1034.8 \pm 57.5 \text{HV}_{0.3}$, and $1136 \pm 26.8 \text{HV}_{0.3}$, respectively. The

average fracture toughness of WC-17Co coatings formed in HVOF, WS, and CS was 8.88 ± 0.31 , 10.42 ± 0.28 , and 13.18 ± 0.49 MPa·m^{-1/2}, respectively.

- V. The main wear mechanism of all coatings was the groove and some peel-offs. The average weight loss of the WC-17Co coatings formed in HVOF, WS, and CS was 8.15 ± 0.31 mg, 5.31 ± 0.32 mg, and 4.05 ± 0.41 mg, respectively. However, the average weight loss of Q235 steel was 21.77 ± 0.25 mg, which was more than 5 times that of the cold-sprayed WC-17Co coating.

Author Contributions: Conceptualization, X.C.; Methodology, X.C. and C.L.; Software, Q.G.; Validation, X.C. and X.D.; Formal Analysis, X.C.; Investigation, H.L.; Resources, X.C.; Data Curation, X.C. and H.L.; Writing—Original Draft Preparation, X.C.; Writing—Review and Editing, C.L.; Visualization, Q.G.; Supervision, X.D.; Project Administration, X.C.; Funding Acquisition, X.C. All authors have read and agreed to the published version of the manuscript.

Funding: This research was funded by National Science Foundation of China, grant number 52161018, the Science and Technology Project of Jiangxi Educational Bureau, grant number GJJ191068, GJJ212304, GJJ212307, and the Science Technology Project of Jiujiang City, grant number [2015] No.64.

Institutional Review Board Statement: Not applicable.

Informed Consent Statement: Not applicable.

Data Availability Statement: Not applicable.

Conflicts of Interest: The authors declare no conflict of interest.

References

- Magnani, M.; Suegama, P.H.; Espallargas, N. Influence of HVOF parameters on the corrosion and wear resistance of WC-Co coatings sprayed on AA7050 T7. *Surf. Coat. Technol.* **2008**, *202*, 4746–4757. [\[CrossRef\]](#)
- Katiyar, P.K.; Singh, P.K.; Singh, R.; Kumar, A. Modes of failure of cemented tungsten carbide tool bits (WC/Co): A study of wear parts. *Int. J. Refract. Met. Hard Mater.* **2016**, *54*, 27–38. [\[CrossRef\]](#)
- Ding, Z.; Chen, W.; Wang, C. Resistance of cavitation erosion of multimodal WC-12Co coatings sprayed by HVOF. *Trans. Nonferrous Met. Soc. China* **2011**, *21*, 2231–2236. [\[CrossRef\]](#)
- Ma, N.; Cheng, Z.X.; Wu, H.T.; Ye, F.X. Effects of structure of feedstock powders on the microstructure and properties of HVOF sprayed WC-Co coatings. *Rare Met. Mat. Eng.* **2015**, *44*, 3219–3223.
- Sahraoui, T.; Fenineche, N.E.; Montavon, G.; Coddet, C. Alternative to chromium: Characteristics and wear behavior of HVOF coatings for gas turbine shafts repair (heavy-duty). *J. Mater. Process. Technol.* **2004**, *152*, 43–55. [\[CrossRef\]](#)
- Ghadami, F.; Sohi, M.H.; Ghadami, S. Effect of TIG surface melting on structure and wear properties of air plasma-sprayed WC-Co coatings. *Surf. Coat. Technol.* **2015**, *261*, 108–113. [\[CrossRef\]](#)
- Balamurugan, G.M.; Duraiselvam, M.; Anandakrishnan, V. Comparison of high temperature wear behaviour of plasma sprayed WC-Co coated and hard chromium plated AISI 304 austenitic stainless steel. *Mater. Des.* **2012**, *35*, 640–646. [\[CrossRef\]](#)
- Bonache, V.; Salvador, M.D.; García, J.C.; Sánchez, E.; Bannier, E. Influence of plasma intensity on wear and erosion resistance of conventional and nanometric WC-Co coatings deposited by APS. *J. Therm. Spray Technol.* **2011**, *20*, 549–559. [\[CrossRef\]](#)
- Chen, H.; Gou, G.Q.; Tu, M.J.; Liu, Y. Research on the friction and wear behavior at elevated temperature of plasma-sprayed nanostructured WC-Co coatings. *J. Mater. Eng. Perform.* **2010**, *19*, 1–6. [\[CrossRef\]](#)
- Zhan, Q.; Yu, L.G.; Ye, F.X.; Xue, Q.J.; Li, H. Quantitative evaluation of the decarburization and microstructure evolution of WC-Co during plasma spraying. *Surf. Coat. Technol.* **2012**, *206*, 4068–4074. [\[CrossRef\]](#)
- Wood, R.J.K. Tribology of thermal sprayed WC-Co coatings. In special issue: Tribology of Hard Coatings. *Int. J. Refract. Met. Hard Mater.* **2009**, *28*, 82–94. [\[CrossRef\]](#)
- Fedrizzi, L.; Valentinelli, L.; Rossi, S.; Segna, S. Tribocorrosion behaviour of HVOF cermet coatings. *Corros. Sci.* **2007**, *49*, 2781–2799. [\[CrossRef\]](#)
- Ding, X.; Ke, D.; Yuan, C.Q.; Ding, Z.X.; Cheng, X.D. Microstructure and cavitation erosion resistance of HVOF deposited WC-Co coatings with different size WC. *Coatings* **2018**, *8*, 307. [\[CrossRef\]](#)
- Mi, P.B.; Zhao, H.J.; Wang, T.; Ye, F.X. Sliding wear behavior of HVOF sprayed WC-(nano-WC-Co) coating at elevated temperatures. *Mater. Chem. Phys.* **2018**, *206*, 1–6. [\[CrossRef\]](#)
- Shipway, P.H.; McCartney, D.G.; Sudaprasert, T. Sliding wear behaviour of conventional and nanostructured HVOF sprayed WC-Co coatings. *Wear* **2005**, *259*, 820–827. [\[CrossRef\]](#)
- Cho, T.Y.; Yoon, J.H.; Kim, K.S.; Song, K.O.; Joo, Y.K.; Fang, W.; Zhang, S.H.; Youn, S.J.; Chun, H.G.; Hwang, S.Y. A study on HVOF coatings of micron and nano WC-Co powders. *Surf. Coat. Technol.* **2008**, *202*, 5556–5559. [\[CrossRef\]](#)

17. Guilemany, J.M.; Dosta, S.; Miguel, J.R. The enhancement of the properties of WC-Co HVOF coatings through the use of nanostructured and microstructured feedstock powders. *Surf. Coat. Technol.* **2006**, *201*, 1180–1190. [[CrossRef](#)]
18. Baumann, I.; Hagen, L.; Tillmann, W.; Hollingsworth, P.; Stangier, D.; Schmidtman, G.; Tolan, M.; Paulus, M.; Sternemann, C. Process characteristics, particle behavior and coating properties during HVOF spraying of conventional, fine and nanostructured WC-12Co powders. *Surf. Coat. Technol.* **2021**, *405*, 126716. [[CrossRef](#)]
19. Mi, P.B.; Ye, F.X. Structure and wear performance of the atmospheric heat-treated HVOF sprayed bimodal WC-Co coating. *Int. J. Refract. Met. Hard Mater.* **2018**, *76*, 185–191. [[CrossRef](#)]
20. Ribu, D.C.; Rajesh, R.; Thirumalaikumarasamy, D.; Kaladgi, R.A.; Saleel, A.C.; Nisar, S.K.; Shaik, S.; Afzal, A. Experimental investigation of erosion corrosion performance and slurry erosion mechanism of HVOF sprayed WC-10Co coatings using design of experiment approach. *J. Mater. Res. Technol.* **2022**, *18*, 293–314. [[CrossRef](#)]
21. Kuroda, S.; Watanabe, M.; Kim, K.; Katanoda, H. Current status and future prospects of warm spray technology. *J. Therm. Spray Technol.* **2011**, *20*, 653–676. [[CrossRef](#)]
22. Watanabe, M.; Brauns, C.; Komatsu, M.; Kuroda, S.; Gärtner, F.; Klassen, T.; Katanoda, H. Effect of nitrogen flow rate on microstructures and mechanical properties of metallic coatings by warm spray deposition. *Surf. Coat. Technol.* **2013**, *232*, 587–599. [[CrossRef](#)]
23. Kawakita, J.; Kuroda, S.; Fukushima, T.; Katanoda, H.; Matsuo, K.; Fukanuma, H. Dense titanium coatings by modified HVOF spraying. *Surf. Coat. Technol.* **2006**, *201*, 1250–1255. [[CrossRef](#)]
24. He, D.; Kusano, M.; Watanabe, M. Detecting the defects of warm-sprayed Ti-6Al-4V coating using Eddy current testing method. *NDT E Int.* **2022**, *125*, 102565. [[CrossRef](#)]
25. Yao, H.L.; Ji, G.C.; Chen, Q.Y.; Bai, X.B.; Zou, Y.L.; Wang, H.T. Microstructures and properties of warm-sprayed carbonated hydroxyapatite coatings. *J. Therm. Spray Technol.* **2018**, *27*, 924–937. [[CrossRef](#)]
26. Ji, G.C.; Zou, Y.L.; Chen, Q.Y.; Yao, H.L.; Bai, X.B.; Yang, C.; Wang, H.T.; Wang, F. Mechanical properties of warm sprayed HATI bio-ceramic composite coatings. *Ceram. Int.* **2020**, *46*, 27021–27030. [[CrossRef](#)]
27. Sienkiewicz, J.; Kuroda, S.; Murakami, H.; Araki, H.; Giżyński, M.; Kurzydłowski, K.J. Fabrication and oxidation resistance of TiAl matrix coatings reinforced with silicide precipitates produced by heat treatment of warm sprayed coatings. *J. Therm. Spray Technol.* **2018**, *27*, 1165–1176. [[CrossRef](#)]
28. Chivavibul, P.; Watanabe, M.; Kuroda, S.; Kawakita, J.; Komatsu, M.; Sato, K.; Kitamura, J. Effect of powder characteristics on properties of warm-sprayed WC-Co coatings. *J. Therm. Spray Technol.* **2010**, *19*, 81–88. [[CrossRef](#)]
29. Chivavibul, P.; Watanabe, M.; Kuroda, S.; Kawakita, J.; Komatsu, M.; Sato, K.; Kitamura, J. Development of WC-Co coatings deposited by warm spray process. *J. Therm. Spray Technol.* **2008**, *17*, 750–756. [[CrossRef](#)]
30. Wesmann, J.A.R.; Espallargas, N. Elucidating the complex role of surface oxides formed during sliding of self-mated warm sprayed WC-CoCr in different environments. *Tribol. Int.* **2016**, *94*, 360–372. [[CrossRef](#)]
31. Watanabe, M.; Komatsu, M.; Kuroda, S. Multilayered WC-Co/Cu coatings by warm spray deposition. *Surf. Coat. Technol.* **2011**, *205*, 5358–5368. [[CrossRef](#)]
32. Watanabe, M.; Komatsu, M.; Kuroda, S. WC-Co/Al multilayer coatings by warm spray deposition. *J. Therm. Spray Technol.* **2012**, *21*, 597–608. [[CrossRef](#)]
33. Li, W.Y.; Cao, C.C.; Yin, S. Solid-state cold spraying of Ti and its alloys: A literature review. *Prog. Mater. Sci.* **2020**, *110*, 100633. [[CrossRef](#)]
34. Couto, M.; Dosta, S.; Torrell, M.; Fernández, J.; Guilemany, J.M. Cold spray deposition of WC-17 and 12Co cermets onto aluminum. *Surf. Coat. Technol.* **2013**, *235*, 54–61. [[CrossRef](#)]
35. Yin, S.; Ekoi, E.J.; Lupton, T.L.; Dowling, D.P.; Lupoi, R. Cold spraying of WC-Co-Ni coatings using porous WC-17Co powders: Formation mechanism, microstructure characterization and tribological performance. *Mater. Des.* **2017**, *126*, 305–313. [[CrossRef](#)]
36. Suo, X.; Yin, S.; Li, H.; Lupoi, R. Numerical and experimental investigation on bonding behavior of cold sprayed porous WC-17Co particles onto different substrates. *Coatings* **2018**, *8*, 367. [[CrossRef](#)]
37. Ang, A.S.M.; Berndt, C.C.; Cheang, P. Deposition effects of WC particle size on cold sprayed WC-Co coatings. *Surf. Coat. Technol.* **2011**, *205*, 3260–3267. [[CrossRef](#)]
38. Li, C.J.; Yang, G.J.; Gao, P.H.; Ma, J.; Wang, Y.Y.; Li, C.X. Characterization of nanostructured WC-Co deposited by cold spraying. *J. Therm. Spray Technol.* **2007**, *16*, 1011–1020. [[CrossRef](#)]
39. Gao, P.H.; Li, C.J.; Yang, G.J.; Li, Y.G.; Li, C.X. Influence of substrate hardness transition on built-up of nanostructured WC-12Co by cold spraying. *Appl. Surf. Sci.* **2010**, *256*, 2263–2268. [[CrossRef](#)]
40. Yang, G.J.; Gao, P.H.; Li, C.X.; Li, C.J. Mechanical property and wear performance dependence on processing condition for cold-sprayed WC-(nanoWC-Co). *Appl. Surf. Sci.* **2015**, *332*, 80–88. [[CrossRef](#)]
41. Ji, G.C.; Wang, H.T.; Chen, X.; Bai, X.B.; Dong, Z.X.; Yang, F.G. Characterization of cold-sprayed multimodal WC-12Co coating. *Surf. Coat. Technol.* **2013**, *235*, 536–543. [[CrossRef](#)]
42. Wang, H.T.; Chen, X.; Bai, X.B.; Ji, G.C.; Dong, Z.X.; Yi, D.L. Microstructure and properties of cold sprayed multimodal WC-17Co deposits. *Int. J. Refract. Met. Hard Mater.* **2014**, *45*, 196–203. [[CrossRef](#)]
43. Niihara, K.; Morena, R.; Hasselman, D.P.H. Evaluation of K_{IC} of brittle solids by the indentation method with low crack-to-indent ratios. *J. Mater. Sci. Lett.* **1982**, *1*, 13–16. [[CrossRef](#)]

44. Marshall, D.B.; Noma, T.; Evans, A.G. A simple method for determining elastic-modulus-to-hardness ratios using Knoop indentation measurements. *J. Am. Ceram. Soc.* **1982**, *65*, 175–176. [[CrossRef](#)]
45. Chen, X.; Wang, H.T.; Ji, G.C.; Bai, X.B.; Fu, W. Microstructure and properties of TiB₂-Ni coatings with different binder phase contents deposited by HVOF spray process. *Rare Met.* **2015**, *41*, 1385–1393. [[CrossRef](#)]
46. Li, W.Y.; Jiang, R.R.; Huang, C.J.; Zhang, Z.H.; Feng, Y. Effect of cold sprayed Al coating on mechanical property and corrosion behavior of friction stir welded AA2024-T351 joint. *Mater. Des.* **2015**, *65*, 757–761. [[CrossRef](#)]
47. Lima, R.S.; Karthikeyan, J.; Kay, C.M.; Lindemann, J.; Berndt, C.C. Microstructural characteristics of cold-sprayed nanostructured WC-Co coatings. *Thin Solid Films.* **2002**, *416*, 129–135. [[CrossRef](#)]
48. Lee, C.W.; Han, J.H.; Yoon, J.; Shin, M.C.; Kwun, S.I. A study on powder mixing for high fracture toughness and wear resistance of WC-Co-Cr coatings sprayed by HVOF. *Surf. Coat. Technol.* **2010**, *204*, 2223–2229. [[CrossRef](#)]
49. Chen, C.; Guo, Z.X.; Li, S.H.; Xiao, Y.; Chai, B.B.; Liu, J.B. Microstructure and properties of WC-17Co cermets prepared using different processing routes. *Ceram. Int.* **2019**, *45*, 9203–9210. [[CrossRef](#)]